

# Sliding-Mode Bilateral Teleoperation Control Design for Master-Slave Pneumatic Servo Systems

R. Moreau<sup>1</sup>, M.T. Pham<sup>1</sup>, M. Tavakoli<sup>2</sup>, M.Q. Le<sup>1</sup>, T. Redarce<sup>1</sup>

<sup>1</sup>Laboratoire Ampère, UMR CNRS 5005, Université de Lyon, INSA-Lyon, F-69621 Villeurbanne Cedex, France

<sup>2</sup>Department of Electrical and Computer Engineering, University of Alberta, Edmonton, AB T6G2V4, Canada

## Abstract

This paper presents a novel bilateral control design scheme for pneumatic master-slave teleoperation systems that are actuated by low-cost solenoid valves. The motivation for using pneumatic actuators in lieu of electrical actuators is that the former has higher force to mass ratio than the latter and is inert to magnetic fields, which is crucial in certain teleoperation applications such as MRI-guided, robot-assisted surgery. A sliding mode approach, called the *three-mode control scheme*, is incorporated into a two-channel bilateral teleoperation architecture, which can implement a position–position, force–force, or force–position scheme. An analysis of stability and transparency of the closed-loop teleoperation system is carried out. The proposed control design performance is experimentally verified on a single-degree-of-freedom pneumatic teleoperation system actuated by on/off valves. Experimental results show high accuracies in terms of position and force tracking under free-space motion and hard-contact motion in the teleoperation system. Another purpose of this paper is to demonstrate the possibility to improve the valve lifetime by increasing the number of control levels. To do this, a new control design, called the *five-mode control scheme*, is developed and compared with the three-mode scheme in time domain as well as in frequency domain.

*Keywords:* Pneumatic actuator, on/off solenoid valve, sliding mode control, bilateral teleoperation, stability, transparency.

## 1. Introduction

A telerobotic system allows a human operator to perform manipulation or sensing tasks in remote, hazardous or confined environments. A bilateral teleoperation system consists of a slave (remote) robot and a master (local robot). The master is handled by the human operator for controlling the slave robot and sensing the slave/environment contact forces. Bilateral teleoperation systems have many promising applications especially in minimally invasive surgery and space and underwater exploration, or hazardous environments where human action is clearly restricted (Maurette et al., 1997; Sabater et al., 2006; Ross et al., 2009; Sanchez et al., 2012).

Transparency is the principal performance goal in bilateral teleoperation controller design (Lawrence, 1993) . It

measures the quality of recreation of the mechanical properties of the remote environment for the human operator. Abundant control theories have been proposed to achieve high teleoperation transparency when the slave is in free motion and/or contact motion. For an overview of control approaches in teleoperation systems, the reader is referred to (Stassen and Smets, 1997; Hokayem and Spong, 2006). Also, quantitative performance comparisons between different teleoperation control methods were reported in (Arcara and Melchiorri, 2002; Aliaga et al., 2004). It has been shown that adding force feedback to a teleoperation system emphasizes the sense of telepresence, and improves the user's ability to perform complex tasks (Sheridan, 1995). Position-position and force-position schemes are examples of conventional bilateral controllers commonly used in practice (Salcudean et al., 2000; Fite et al., 2001; Kim et al., 2005).

Besides transparency, stability is also a key issue in the control of bilateral teleoperation systems. Energetic passivity of teleoperation systems has been widely used to ensure human-robot interaction safety. Indeed, implementing each component of a teleoperation system (e.g., the master, the slave, the communication channel, etc.) as a passive element and interconnecting them in a power preserving way leads to a passive system, which is consequently characterized by a stable behavior. Several passivity based strategies have been proposed for teleoperators such as those in (Anderson and Spong, 1989; Niemeyer and Slotine, 1991; Stramigioli et al., 2002; Lee and Li, 2003).

In certain applications involving bilateral teleoperation, the master and the slave robots work at different power scales (e.g., microsurgery or telemanipulation with a large-scale slave robot for extra-vehicular activity in space applications). Several researchers have addressed this problem, resulting in control algorithms that improve the performance of the teleoperation system in a way that is compatible with the velocity/force scaling. For instance, (Itoh et al., 2000) proposed a control law based on a cancellation of the open-loop nonlinear dynamics, which was replaced by a desired virtual tool dynamics. (Lee and Li, 2005) decomposed a teleoperation system into a shape and a locked system in order to implement scaled coordination between master and slave robots. This control scheme allowed to render the closed-loop teleoperator as a common passive mechanical tool with which both the human and the environment interact, and whose inertia and dynamics can be adjusted according to a given task objective.

Commonly, the actuators used in most of teleoperation systems are electrical direct-current motors. They are easy to install, quiet, and simple to control. However, when gear-boxes are used to produce large actuation torques, they may result in backlash and high inertia, which are undesirable because they introduce discontinuity and distortion in the force reflected to the operator. In this study, we investigate the development and control of pneumatic actuators in a teleoperation system. Compared to the electrical actuators, pneumatic actuators have higher force-to-mass ratio and can

generate larger forces without the need for any reduction mechanism such as a gear-box. Moreover, they are inert to magnetic field, which is crucial in certain applications such as robot-assisted surgery under MRI guidance (Ningbo Yu et al., 2008).

Due to the above advantages, pneumatic actuators have found use in various applications of bilateral teleoperation. For instance, (Ben-Dov and Salcudean, 1993) presented force-reflecting control of a 6-DOF haptic master actuated by flapper servovalves and low-friction cylinders. More recently, (Tadano and Kawashima, 2007) proposed a forceps manipulator for a surgical master-slave system capable of estimating external forces without using any force sensor. (Durbha and Li, 2009) proposed a passive bilateral teleoperation system with human power amplification through pneumatic actuators. The input human force was amplified through the pneumatic teleoperator to provide assistance for the human operator in terms of performing the task. This would help the human operator to perform tasks that required high force or power such as lifting a heavy object. (Guerriero and Book, 2008) controlled the foot positions of two 3-DOF legged slave robots driven by pneumatic actuators. In this system, bilateral teleoperation provided force feedback to the operator through two PHANTOM master haptic devices as a function of the foot position error. Pneumatic muscle actuators have been recently used in a teleoperation system (Tondu et al., 2005). These are compact and have high power/weight density actuators that are difficult to control and require accurate experimental characterization.

In some of the recent work involving pneumatic actuation, servovalves rather than solenoid (on/off) valves have been used to achieve high performances in various position control or force control tasks. However, it must be noted that servovalves are typically expensive components as they involve high-precision manufacturing. Therefore, in this paper, fast-switching on/off valves are used due to their additional advantages in terms of low cost and small size over servovalves. One of the objectives of this paper is to show that good teleoperation transparency can be obtained with these inexpensive components as actuators of a teleoperation system.

The traditional control approach for systems with solenoid valves involves using Pulse Width Modulation (PWM) to control the output mass flow rate of the valve (Noritsugu, 1985; Shih and Ma, 1998; Taghizadeh et al., 2009). A main disadvantage of the PWM control is the chattering phenomenon in steady state caused by the high-frequency switching of the valve (Hodgson et al., 2011; Le et al., 2011). Chattering can drastically reduce the valve's lifetime and generate noises that are possibly disturbing for certain applications.

To overcome the drawbacks of PWM-based control of solenoid valves, this paper presents a nonlinear sliding-mode teleoperation control inspired by the scheme used in (Nguyen et al., 2007). The first contribution of our study is to use a

sliding approach in a two-channel bilateral teleoperation with three different architectures, namely position–position, force–force, and force–position. These architectures are chosen due to their implementation simplicity and efficiency. A tracking performance analysis and a stability analysis are provided for the closed-loop system using a Lyapunov candidate function. Another contribution of our work is extending the sliding mode strategy based on the three-mode control scheme (3MCS) to a five-mode control scheme (5MCS). This new scheme results in reduced valve-switching activity and, therefore, improves the overall lifetime and reliability of the teleoperation system.

For the sake of simplicity, the master and slave actuators are considered to be identical in this study – indeed, the master and the slave are one-degree-of-freedom (DOF) manipulators with pneumatic on/off actuation. It should be noted that this paper does not consider the possible presence of time delays in the teleoperation system’s communication channel – for time delay compensation in haptic teleoperation, the readers may refer to (Aziminejad et al., 2008; Chopra et al., 2008). Such delays are commonly present in long-distance teleoperation systems but are generally negligible in local teleoperation systems. It is noteworthy that local teleoperation systems are currently more common than long-distance teleoperation systems and have applications such as minimally invasive surgery, scaled teleoperation for dexterity enhancement.

This paper is organized as follows. Section 2 presents the dynamical model of the pneumatic manipulator. Section 3 describes the implementation of a three-mode control scheme in a two-channel master-slave telemanipulation system. To evaluate the proposed controller performance, experimental results as well as data analysis and interpretation appear in Section 4. Section 5 presents the extension of the three-mode scheme to the five-mode scheme. A comparison of both schemes is also carried out in this section. Finally, Section 6 draws conclusions and highlights the future works.

## **2. Modeling of the Pneumatic System**

As mentioned above, the master and the slave manipulators are identical, thus only one pneumatic robot is presented in this section. To describe the air flow dynamics in a cylinder, we assume that

- air is a perfect gas and its kinetic energy is negligible in the chamber,
- the pressure and the temperature are homogeneous in each chamber,
- the evolution of the gas in each chamber is polytropic,
- the temperature variation in chambers is negligible with respect to the supply temperature,
- the mass flow rate leakages are negligible, and

- the supply and exhaust pressures are constant.

A schematic of the 1-DOF pneumatic actuation system is shown in Fig. 1. The device consists of a pneumatic cylinder, four solenoid valves, a force sensor, and a position sensor. Each chamber is connected to two solenoid valves, where valves 1 and 4 are connected to the supply pressure while valves 2 and 3 are connected to the atmosphere pressure.

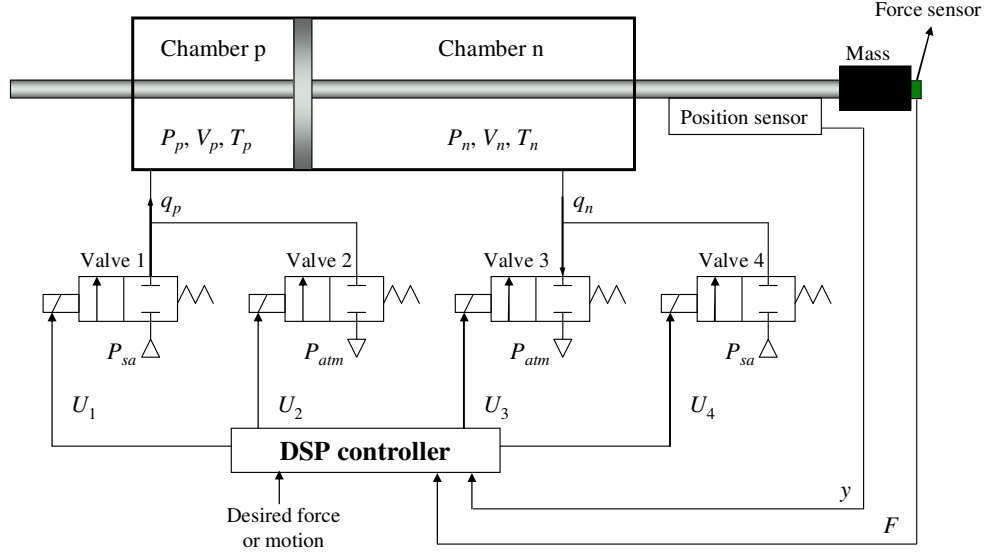


Fig. 1. Electro-pneumatic system with four valves

The behavior of the pressure inside each chamber of the cylinder can be expressed as (Blackburn, 1960)

$$\begin{aligned} \dot{P}_p &= \frac{\gamma r T_a}{V_p(y)} \left( q_p(U_1, U_2, P_p) - \frac{P_p}{r T_a} S_p \dot{y} \right) \\ \dot{P}_n &= \frac{\gamma r T_a}{V_n(y)} \left( q_n(U_3, U_4, P_n) + \frac{P_n}{r T_a} S_n \dot{y} \right) \end{aligned} \quad (1)$$

where  $U_1$ ,  $U_2$ ,  $U_3$  and  $U_4$  are the discrete control voltages (1 or 0) of valve 1, valve 2, valve 3, and valve 4,  $y$  and  $\dot{y}$  are the position (m) and velocity (m/s) of the piston,  $P_p$  and  $P_n$  are the pressures inside chambers p and n (Pa),  $V_p$  and  $V_n$  are the volumes of chambers p and n ( $m^3$ ),  $S_p$  and  $S_n$  are the piston cylinder area in the chambers p and n ( $m^2$ ),  $q_p$  and  $q_n$  are the mass flow rates in chambers p and n (kg/s),  $T_a$  is the temperature of the supply air (K),  $r$  is the perfect gas constant (J/(kg.K)) and  $\gamma$  is the polytropic constant.

The mass flow rate characteristics of the on/off valves can be expressed as functions of the discrete control voltages and the pressures:

$$\begin{aligned}
q_p(U_1, U_2, P_p) &= \begin{cases} q_m(P_{sa}, P_p) & \text{for } U_1=1 \text{ and } U_2=0 \text{ (chamber p fills)} \\ 0 & \text{for } U_1=0 \text{ and } U_2=0 \text{ (chamber p closes)} \\ -q_m(P_p, P_{atm}) & \text{for } U_1=0 \text{ and } U_2=1 \text{ (chamber p exhausts)} \end{cases} \\
q_n(U_3, U_4, P_n) &= \begin{cases} q_m(P_{sa}, P_p) & \text{for } U_3=0 \text{ and } U_4=1 \text{ (chamber n fills)} \\ 0 & \text{for } U_3=0 \text{ and } U_4=0 \text{ (chamber n closes)} \\ -q_m(P_p, P_{atm}) & \text{for } U_3=1 \text{ and } U_4=0 \text{ (chamber n exhausts)} \end{cases}
\end{aligned} \tag{2}$$

where  $P_{sa}$  and  $P_{atm}$  are the pressures of the supply air and atmosphere. The ‘0’ state of the input voltage corresponds to a closed valve and the ‘1’ state corresponds to an open valve. All the states where  $U_1 = U_2 = 1$  and  $U_3 = U_4 = 1$  are prohibited to avoid a bypass of the valves. The functions in (2) are given by a standard expression in which the mass flow rate of the valve is regulated by the air passage through an orifice (McCloy, 1968):

$$q(P_{up}, P_{down}) = \begin{cases} C_{val} P_{up} \sqrt{\frac{T_{atm}}{T_{up}}} & \text{if } \frac{P_{down}}{P_{up}} \leq 0.433 \text{ (sonic)} \\ C_{val} P_{up} \sqrt{\frac{T_{atm}}{T_{up}}} \sqrt{1 - \left( \frac{\frac{P_{down} - C_r}{P_{up}}}{1 - C_r} \right)^2} & \text{otherwise (subsonic)} \end{cases} \tag{3}$$

In the above expression,  $C_{val}$  is the valve flow rate coefficient,  $C_r$  is the critical pressure ratio,  $P_{up}$  and  $P_{down}$  are respectively the absolute upstream and downstream stagnation pressures of the valve (Pa),  $T_{atm}$  is the atmosphere temperature, and  $T_{up}$  is the upstream stagnation temperature.

Finally, the dynamics of the piston and the load are

$$M\ddot{y} = S_p P_p - S_n P_n - b\dot{y} - F_{st} + F_{ext} \tag{4}$$

where  $b$  is the viscous friction coefficient (N.s/m),  $M$  is the moving load (kg),  $F_{st}$  is the stiction force (N), and  $F_{ext}$  is the external force (N). For simplicity, the stiction force is assumed to be negligible.

### 3. Teleoperation Based on Sliding Control

In order to facilitate the control law design, a switching scheme for the four solenoid valves in Fig. 1 is defined so that each of the master and slave robots has the three modes of operation shown in Table I.

TABLE I: THREE POSSIBLE CONTROL MODES

	Mode 1	Mode 2	Mode 3
Chamber p	fills	exhausts	closed
Chamber n	exhausts	fills	closed
Control $u$	1	-1	0
$U = [U_1 U_2 U_3 U_4]$	[1 0 1 0]	[0 1 0 1]	[0 0 0 0]

Here,  $U$  (the 4<sup>th</sup> row) is defined as the input voltage vector of the valves. Also,  $u$  (the 3<sup>rd</sup> row) is a newly introduced discrete (switching) control input that has three levels to match the three modes of operation. This new input can be chosen either as  $u = \text{sign}(s)$  or  $u = -\text{sign}(s)$ , where  $s$  is the sliding surface and is a measure of tracking error. The exact choice of the switching control  $u$  depends on the definition of the sliding surface  $s$ . As it will be shown later, this choice is crucial to ensuring the stability of the teleoperation system.

Note that modes 1 and 2 in Table I are used for changing the direction of the force on the piston, and mode 3 is used to save energy and reduce the chattering phenomenon when the tracking error is small enough. In order to bring the system to the sliding surface  $s = 0$  at steady state, which corresponds to perfect tracking performance, we define a neighbourhood of radius  $\varepsilon \ll 1$  around zero. When  $|s|$  is within this neighbourhood, the third mode ( $u = 0$ ) is used to conserve energy and somewhat reduce chattering. In summary, in general the control law takes the form

$$u = \begin{cases} +/\text{-sign}(s) & \text{if } |s| > \varepsilon \\ 0 & \text{if } |s| \leq \varepsilon \end{cases} \quad (5)$$

### 3.1. Open-loop Models of Master and Slave manipulators

Ignoring the stiction force in (4), the mechanical dynamics of the master and slave manipulators can be written as

$$\begin{aligned} M\ddot{y}_m &= S_p P_{p,m} - S_n P_{n,m} - b\dot{y}_m + f_h \\ M\ddot{y}_s &= S_p P_{p,s} - S_n P_{n,s} - b\dot{y}_s - f_e \end{aligned} \quad (6)$$

where  $f_h$  and  $f_e$  are the operator force exerted on the master and the environment force exerted on the slave, and  $y_m$  and  $y_s$  are the master and slave positions. Differentiating (6) and using (1)–(2), the dynamics of the master and slave manipulators are obtained after some calculations (Nguyen et al., 2007):

$$\ddot{y}_m = \begin{cases} \alpha_m + \beta_m^+ + \dot{f}_h/M, & u_m = 1 \\ \alpha_m - \beta_m^- + \dot{f}_h/M, & u_m = -1, \\ \alpha_m + \dot{f}_h/M, & u_m = 0 \end{cases}, \quad \ddot{y}_s = \begin{cases} \alpha_s + \beta_s^+ - \dot{f}_e/M, & u_s = 1 \\ \alpha_s - \beta_s^- - \dot{f}_e/M, & u_s = -1 \\ \alpha_s - \dot{f}_e/M, & u_s = 0 \end{cases} \quad (7)$$

where  $u_m$  and  $u_s$  denote the discrete control input as defined in Table I. In the above,

$$\alpha_i = -\frac{b}{M} \ddot{y}_i - \frac{\gamma}{M} \left( \frac{S_p^2 P_{p,i}}{V_p(y_i)} + \frac{S_n^2 P_{n,i}}{V_n(y_i)} \right) \dot{y}_i \quad (8)$$

$$\beta_i^+ = \gamma r T_a \left( \frac{S_p}{M} \frac{q(P_{sa}, P_{p,i})}{V_p(y_i)} + \frac{S_n}{M} \frac{q(P_{n,i}, P_{atm})}{V_n(y_i)} \right) \quad (9)$$

$$\beta_i^- = \gamma r T_a \left( \frac{S_p}{M} \frac{q(P_{p,i}, P_{atm})}{V_p(y_i)} + \frac{S_n}{M} \frac{q(P_{sa}, P_{n,i})}{V_n(y_i)} \right) \quad (10)$$

with  $i = m$  or  $s$  (for master or slave, respectively).

### 3.2. Closed-loop Teleoperation System

In this subsection, the sliding mode control is applied to a two-channel bilateral teleoperation architecture with various schemes (i.e., position-position, force-force, and force-position schemes). It is noteworthy that there exist more complex teleoperation control architectures, e.g., 4-channel and 3-channel schemes, which involve the transfer of more information (force and position) from/to the master and the slave (Zhu and Salcudean, 1995; Hashtrudi-Zaad and Salcudean, 2001; Tavakoli et al., 2007). More complex control architectures may be needed for multilateral cooperative teleoperation, which involve multiple master robots and/or multiple slave robots. There are three classes of such systems reported in the literature, i.e., *single-master/multiple-slave*, *multiple-master/single-slave*, and *multiple-master/multiple-slave*. The implementation of the sliding mode control in such architectures is more complicated than the 2-channel framework proposed in our study. However, it was chosen for the simplicity of the control validation.

#### 3.2.1. Position Error Based (PEB) Control

A position-error-based, also called position-position, teleoperation system involves the simplest bilateral controller in which no force sensors are required. This architecture involves the transmission of two signals between the master and the slave: position (or velocity) from the master to the slave and vice versa. The aim of this architecture is to minimize the difference between the master and the slave positions (Anderson and Spong, 1989; Salcudean et al., 1995; Fite et al., 2001; Aliaga et al., 2004). The pneumatic-actuated PEB teleoperation system with our proposed sliding mode control is shown in Fig. 2.

Note that throughout this paper, we use positions instead of velocities in our formalism. This is due to the fact that ensuring velocity tracking between the master and the slave might cause small offsets between the master and slave positions (i.e., steady-state errors in position tracking). Generally, when the delay in the communication channel is negligible, the use of position controllers or velocity controllers does not affect the stability of the teleoperation system, thus we opt to use position controllers (Tavakoli et al., 2007).

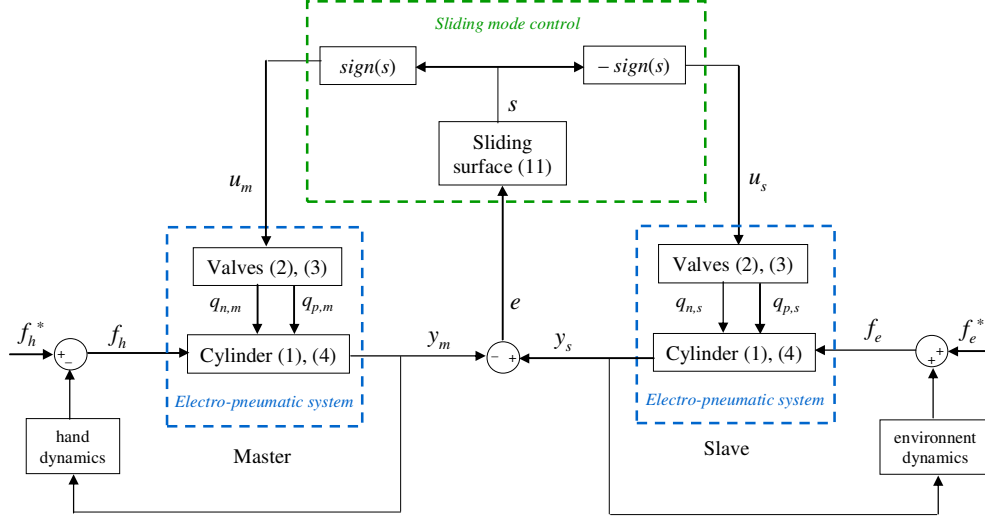


Fig. 2. Position-Error-Based approach with sliding mode control

In Fig. 2,  $s$  is the sliding surface,  $u_m$  and  $u_s$  are the discrete control signals for the master and the slave manipulators, and  $e = y_s - y_m$  is the position tracking error. Also,  $f_h^*$  and  $f_e^*$  are the operator's and the environment's exogenous input forces, respectively, and are independent of teleoperation system behavior.

In the PEB scheme, the sliding surface  $s$  can be defined as

$$s = \ddot{e} + 2\xi\omega\dot{e} + \omega^2 e \quad (11)$$

where  $e = y_s - y_m$  is the position error between the master and the slave and  $\xi$  and  $\omega$  are constant and positive parameters. The control laws  $u_m$  and  $u_s$  are defined as  $u_s = -u_m = -\text{sign}(s)$ . In the following, we analyze the position error convergence and the stability of the closed-loop system.

Consider the following Lyapunov candidate function

$$V = \frac{1}{2} s^2 \quad (12)$$

The sliding surface  $s = 0$  is reached within a finite time if the following condition is satisfied (Slotine et al., 1991; Utkin and Chang, 2002):

$$\dot{V} = s\dot{s} < -\eta|s| \quad (13)$$

for some constant  $\eta > 0$ . Thus, from (11) and (13), we need

$$s(\ddot{e} + 2\xi\omega\dot{e} + \omega^2 e) < -\eta|s| \quad (14)$$

**Case 1:**  $s > 0$ . In this case, (14) becomes

$$(\ddot{y}_s - \ddot{y}_m) + 2\xi\omega\dot{e} + \omega^2 e < -\eta \quad (15)$$

Since  $s > 0$ , then  $u_s = -1$  and  $u_m = 1$ . Therefore, the master and slave open-loop dynamics in (7) become

$$\ddot{y}_m = \alpha_m + \beta_m^+ \dot{f}_h / M, \quad \ddot{y}_s = \alpha_s - \beta_s^- \dot{f}_e / M \quad (16)$$

Substituting (16) in (15) leads to the following condition

$$(\alpha_s - \alpha_m) - (\beta_m^+ + \beta_s^-) (\dot{f}_h + \dot{f}_e) / M + 2\xi\omega\dot{e} + \omega^2 e < -\eta \quad (17)$$

In other words,

$$\lambda - (\beta_m^+ + \beta_s^-) < -\eta \quad (18)$$

where

$$\lambda = \alpha_s - \alpha_m - (\dot{f}_h + \dot{f}_e) / M + 2\xi\omega\dot{e} + \omega^2 e \quad (19)$$

◆

**Case 2** :  $s < 0$ . In this case, (14) becomes

$$(\ddot{y}_s - \ddot{y}_m) + 2\xi\omega\dot{e} + \omega^2 e > \eta \quad (20)$$

Since  $s < 0$ , then  $u_s = 1$  and  $u_m = -1$ . Hence, the master and slave dynamics in (7) can be expressed as

$$\ddot{y}_m = \alpha_m - \beta_m^- \dot{f}_h / M, \quad \ddot{y}_s = \alpha_s + \beta_s^+ \dot{f}_e / M \quad (21)$$

Substituting (21) in (20) yields

$$\lambda + (\beta_m^- + \beta_s^+) > \eta \quad (22)$$

where  $\lambda$  is defined in (19).

◆

Note that, from (9) and (10),  $\beta_i^+$  and  $\beta_i^-$  are positive, and can be made as large as desired by choosing a sufficiently large valve orifice  $C_{val}$  in (3). Thus, to ensure that the conditions (18) and (22) (depending on the sign of  $s$ ) are satisfied, we only need to show that  $\lambda$  is bounded – note that  $\eta > 0$  is an arbitrary constant.

To show that  $\lambda$  is bounded, we utilize the following dynamic models of the operator and the environment (Oboe and Fiorini, 1998; Yoshikawa and Ichinoo, 2003)

$$\begin{aligned} f_h &= -M_h \ddot{y}_m - B_h \dot{y}_m - K_h y_m + f_h^* \\ f_e &= M_e \ddot{y}_s + B_e \dot{y}_m + K_e y_m + f_e^* \end{aligned} \quad (23)$$

where  $M_h$ ,  $M_e$ ,  $B_h$ ,  $B_e$ ,  $K_h$  and  $K_e$  are assumed to be positive values corresponding to the mass, damping and stiffness of the operator's hand and the environment, respectively. Substituting (23) into the master and the slave dynamics (6) yields

$$\begin{aligned}
(M + M_h)\ddot{y}_m &= S_p P_{p,m} - S_n P_{n,m} - (b + B_h)\dot{y}_m - K_h y_m + f_h^* \\
(M + M_e)\ddot{y}_s &= S_p P_{p,s} - S_n P_{n,s} - (b + B_e)\dot{y}_s - K_e y_s - f_e^*
\end{aligned} \tag{24}$$

To establish the boundedness of  $\lambda$ , we consider the following points:

- Since we are dealing with a physical system, the chamber pressures  $P_{p,i}$  and  $P_{n,i}$  are supposed to be bounded at all times. In fact, they are lower-bounded by the atmospheric pressure ( $P_{atm}$ ) and upper-bounded by the supply pressure ( $P_{sa}$ ).
- The exogenous input forces  $f_h^*$  and  $f_e^*$  and their derivatives are supposed to be bounded as they originate solely from the human operator and the environment, which have limited energy.
- Since the coefficients of position, velocity and acceleration terms in (24) (after moving them to the left side of the equations) are positive, and since the pressures, the operator's and the environment's exogenous force  $f_h^*$  and  $f_e^*$  are always bounded, thus each relationship in (24) is a second order BIBO stable system. As a result, the positions  $y_m$  and  $y_s$  are always bounded. In a similar way, (24) consists two first-order stable differential equations in terms of velocities and the other sides of the equations (consisting of positions, pressures and exogenous forces) are bounded, thus the master's and slave's velocities  $\dot{y}_m$  and  $\dot{y}_s$  are bounded. Hence, again because of (24), the accelerations  $\ddot{y}_m$  and  $\ddot{y}_s$ , which are the sums of bounded functions, are also bounded.
- Since the velocities and the accelerations are bounded, from (6), knowing that the pressures are bounded, we can infer that the interaction forces  $f_h$  and  $f_e$  are also bounded at all times.
- $V_p(y_i)$  and  $V_n(y_i)$ , the chamber volumes of the cylinders, are always bounded and non-zero functions.
- The rate of change of pressures, i.e.,  $\dot{P}_{p,i}$  and  $\dot{P}_{n,i}$ , are bounded at all times because each relationship in (1) is defined by a mass flow rate, a velocity, a pressure, a chamber volume, which are all bounded functions.
- Based on the previous points, differentiating (24) yields the boundedness of  $\ddot{y}_m$  and  $\ddot{y}_s$ . Consequently, by taking the derivative of (23) we infer that  $\dot{f}_h$  and  $\dot{f}_e$  are also bounded at all times.

Eventually, it is found that  $\lambda$ , which is the sum of several bounded functions, is bounded. Consequently, the sliding condition in (13) is ensured at all times, which implies that the position tracking error tends to zero (and that the overall system is stable). In fact, from (13),  $s$  will be bounded and converges to zero. According to (11), which represents a BIBO-stable second-order LTI system, this will ensure the boundedness and convergence to zero of the position tracking error.

A drawback of the PEB method is that it does not guarantee good transparency in term of force tracking. In order to

improve the tracking performance, other schemes are proposed in the next sections.

### 3.2.2. Force Error Based (FEB) Control

A force-error-based, also called force-force, system is not commonly used in two-channel bilateral teleoperation since two force sensors are required, which will make the implementation expensive, and since the resulting position tracking is not good. However, compared to the PEB architecture, this architecture can improve the force tracking performance. Fig. 3 shows the pneumatic-actuated FEB teleoperation system with a proposed sliding mode control.

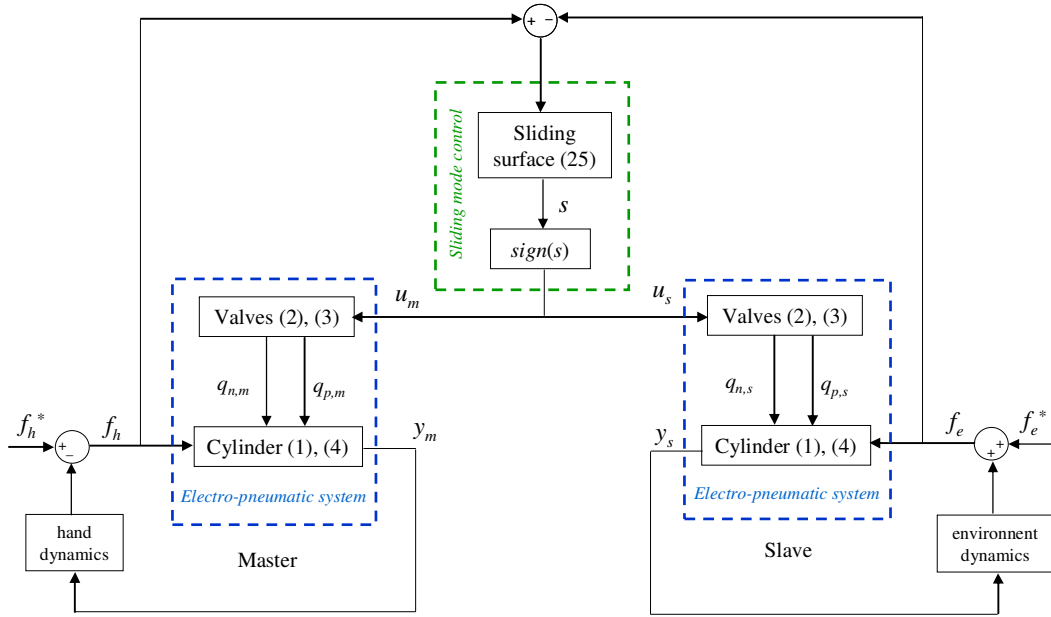


Fig. 3. Force-Error-Based approach with sliding mode control

Consider the control law  $u_s = u_m = \text{sign}(s)$  where the sliding surface is defined as

$$s = f_h - f_e \quad (25)$$

Using the Lyapunov function (12), we need to show that the sliding condition (13) is satisfied. From the master and slave models (7), we calculate  $\dot{f}_h$  and  $\dot{f}_e$  as

$$\dot{f}_h = \begin{cases} M(\ddot{y}_m - \alpha_m - \beta_m^+), & u_m = 1 \\ M(\ddot{y}_m - \alpha_m + \beta_m^-), & u_m = -1 \\ M(\ddot{y}_m - \alpha_m), & u_m = 0 \end{cases}, \quad \dot{f}_e = \begin{cases} M(-\ddot{y}_s + \alpha_m + \beta_s^+), & u_s = 1 \\ M(-\ddot{y}_s + \alpha_m - \beta_s^-), & u_s = -1 \\ M(-\ddot{y}_s + \alpha_m), & u_s = 0 \end{cases} \quad (26)$$

**Case 1:**  $s > 0$ . In this case  $u_m = u_s = 1$ . From (13), we need

$$\dot{s} = \dot{f}_h - \dot{f}_e = M(\lambda - \beta_m^+ - \beta_s^+) < -\eta \quad (27)$$

where

$$\lambda = \ddot{y}_m - \alpha_m + \ddot{y}_s - \alpha_s \quad (28)$$

The condition in (27) can be verified when  $\lambda$ , which is defined in (28), is bounded. As it was demonstrated in section 3.2.1, every signal is bounded, including  $\ddot{y}_m$ ,  $\alpha_m$ ,  $\ddot{y}_s$  and  $\alpha_s$ . This implies the boundedness of  $\lambda$  at all times. Finally, by choosing a valve with a large enough orifice,  $\beta_m^+$  and  $\beta_s^+$  can be made sufficiently large to satisfy (27).

◆

**Case 2:**  $s < 0$ . In this case,  $u_m = u_s = -1$ . We have

$$\dot{s} = \dot{f}_h - \dot{f}_e = M(\lambda + \beta_m^- + \beta_s^-) > \eta \quad (29)$$

where  $\lambda$  is defined in (28).

Similar to Case 1,  $\lambda$  is bounded at all times. Thus, the stability of the system (29) can be guaranteed by choosing a large enough value of  $\beta_m^-$  and  $\beta_s^-$ .

◆

Consequently, the force tracking error converges to zero and the overall system is stable. However, the FEB method does not guarantee a good position tracking performance. In order to overcome the PEB and FEB architecture drawbacks, we use the scheme described in the following section.

### 3.2.3. Direct Force Reflection (DFR) Control

A direct-force-reflection, also called force-position, system has advantages over the position–position and force–force architectures. Compared to the PEB method, improvements in term of force tracking are achieved due to the measurement of the interaction force between the slave and the environment. Furthermore, its position tracking performance is better than the FEB case thanks to position information. The pneumatic-actuated DFR teleoperation system with our proposed sliding mode control is illustrated in Fig. 4.

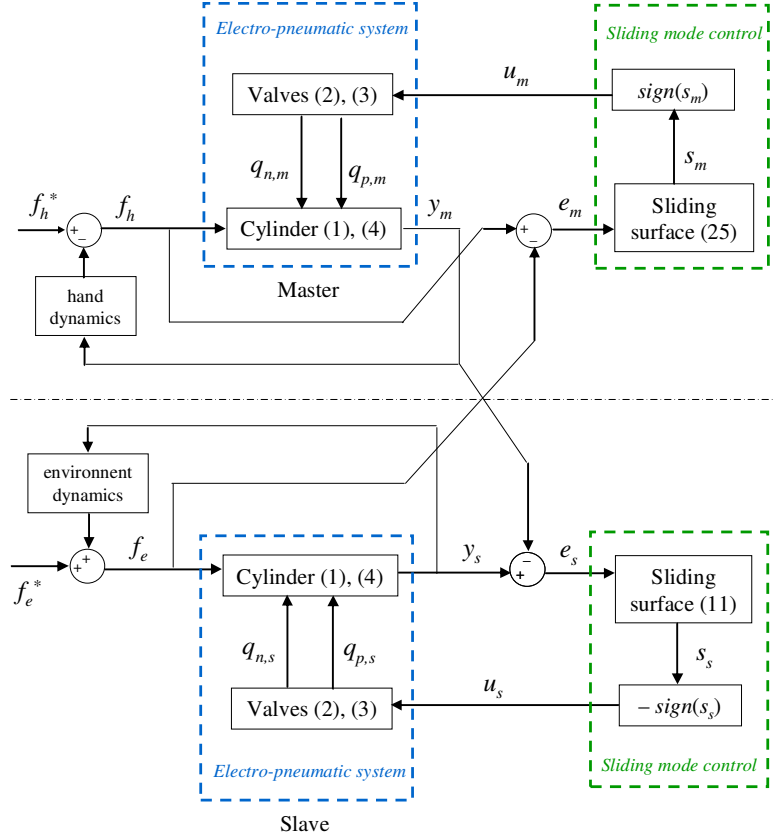


Fig. 4. Direct-Force-Reflection approach with sliding mode control

Here,  $s_m$  and  $s_s$  are the sliding surfaces for the master and slave systems, respectively,  $e_m = f_h - f_e$  is the force tracking error calculated for the master controller, and  $e_s = y_s - y_m$  is the position tracking error calculated for the slave controller. This architecture involves the transmission of two types of data between the master and the slave: force from the slave to master and position from the master to the slave. Hence, the transparency is improved in terms of force and position tracking, compared to these previous methods. This statement will be justified later in our experiment, Section 4.

In this section, we use a Lyapunov function to prove the stability of the sliding-mode controlled DFR system. First, we will show the stability of the force-controlled master manipulator. Afterwards, we will show the stability of the position-controlled slave manipulator. However, the stability of the overall system is difficult to show due to the complexities introduced by using different sliding surfaces for the master and for the slave.

#### a. Force convergence of the closed-loop master system

Since the desired force for the master robot, i.e., the slave/environment contact force  $f_e$  is assumed to be bounded at the beginning, we need to show that  $f_h$  converges to  $f_e$  in a finite time. The sliding surface  $s_m$  and the Lyapunov function  $V_m$  are defined as in (25) and (12), respectively. The controller  $u_m$  is chosen to be similar to the FEB system in section 3.2.2.

**Case 1:**  $s_m > 0$ . In this case,  $u_m = 1$ . Using the expression of  $\dot{f}_h$  in (26) and the definition of  $s_m$  as in (25) we have

$$\dot{s}_m = -\dot{f}_e + M\ddot{y}_m - M\alpha_m - M\beta_m^+ \quad (30)$$

To ensure the sliding condition (13), we need to show that

$$-\dot{f}_e + M\ddot{y}_m - M\alpha_m - M\beta_m^+ < -\eta \quad (31)$$

Similar to how it was demonstrated in section 3.2.1,  $\dot{f}_e$ ,  $\ddot{y}_m$  and  $\alpha_m$  can be shown to be bounded at all times. Thus, the stability condition (31) is satisfied by choosing a large enough value for  $\beta_m^+$ .

◆

**Case 2:**  $s_m < 0$ . In this case,  $u_m = -1$ . From (25) and (26) we need

$$-\dot{f}_e + M\ddot{y}_m - M\alpha_m + M\beta_m^- > \eta \quad (32)$$

Similar to Case 1, it is possible to choose a large enough value of  $\beta_m^-$  in order to ensure the stability of the master device.

◆

Consequently, the sliding surface (the force tracking error) tends to zero, i.e.,  $f_h$  tends towards  $f_e$ .

#### b. Position convergence of the closed-loop slave system

The sliding surface  $s_s$  and the Lyapunov function  $V_s$  are defined as in (11) and (12), respectively. The controller  $u_s$  is chosen to be similar to the PEB system in section 3.2.1.

**Case 1:**  $s_s > 0$ . In this case,  $u_s = -1$ . The sliding condition (13) is equivalent to

$$(\ddot{y}_s - \ddot{y}_m) + 2\xi\omega\ddot{e}_s + \omega^2\dot{e}_s < -\eta \quad (33)$$

Using the expression of  $\ddot{y}_s$  in (16) leads to the following condition

$$\alpha_s - \beta_s^- - \dot{f}_e/M - \ddot{y}_m + 2\xi\omega\ddot{e}_s + \omega^2\dot{e}_s < -\eta \quad (34)$$

or

$$\varphi - \beta_s^- < -\eta \quad (35)$$

where  $\varphi = \alpha_s - \dot{f}_e/M - \ddot{y}_m + 2\xi\omega\ddot{e}_s + \omega^2\dot{e}_s$

The straightforward reasoning described in section 3.2.1 allows us to infer that  $\varphi$  is bounded at all times. Thus, there exists a value of  $\beta_s^-$  such as (33) is satisfied.

◆

**Case 2:**  $s_s < 0$ . In this case,  $u_s = 1$ . Thus, we need

$$\alpha_s + \beta_s^+ - \ddot{y}_m - \dot{f}_e / M + 2\xi\omega\ddot{e}_s + \omega^2\dot{e}_s > \eta \quad (36)$$

or

$$\varphi + \beta_s^+ > \eta \quad (37)$$

This condition is achieved by choosing a large enough  $\beta_s^+$ .

◆

Note that for both cases, the convergence of the sliding surface (and thus the position tracking errors) to zero is proved, so  $x_s$  tends towards  $x_m$ .

Among the different stability analysis methods based on the passivity theory that were mentioned in Section I, this paper has directly studied the stability of the overall teleoperation system, which has the potential to reduce design conservatism and allow for higher teleoperation performance. It should be noted that our stability analysis is achieved when the real-world limits of some system states (i.e., the boundedness of the pressure chambers between the atmosphere pressure and the supply pressure) are taken into account. Showing the stability without using the knowledge on bounded pressures is very difficult because we are dealing with a complex nonlinear, discrete-input pneumatic system.

## 4. Experiments

### 4.1. Experimental Setup

In this section, experiments with a 1-DOF teleoperation system are reported. As illustrated in Fig. 5, the setup consists of two identical pneumatic manipulators (as the master and the slave). The low friction cylinders (Airpel model M16D100D) have a 16 mm diameter and a 100 mm stroke. The pistons are connected to a mass of approximately  $M = 1$  kg. In terms of actuators, each pneumatic cylinder uses four solenoid valves. The pneumatic solenoid valves (Matrix model GNK821213C3K) used to control the air flow have switching times of approximately 1.3 ms (opening time) and 0.2 ms (closing time). With such fast switching times, the on/off valves are appropriate for the purposes of the proposed control. In terms of sensors, a low-friction linear variable differential transformer (LVDT) is connected to each cylinder in order to measure the master's and the slave's linear positions. Also, each of the end-effectors of the master and the slave manipulators is equipped with a force sensor – this will help to measure the operator's and the environment's forces, respectively. The system was supplied with air at an absolute pressure of 300 kPa.

The controller is implemented using a dSPACE board (DS1104), running at a sampling rate of 500 Hz. This value has been chosen according to the open/close bandwidth of the switching valves and to guarantee an acceptable tracking

response. This sampling rate is also higher than the bandwidth above which the human finger cannot distinguish two consecutive force stimuli, which is 320 Hz (Shimoga, 1993).

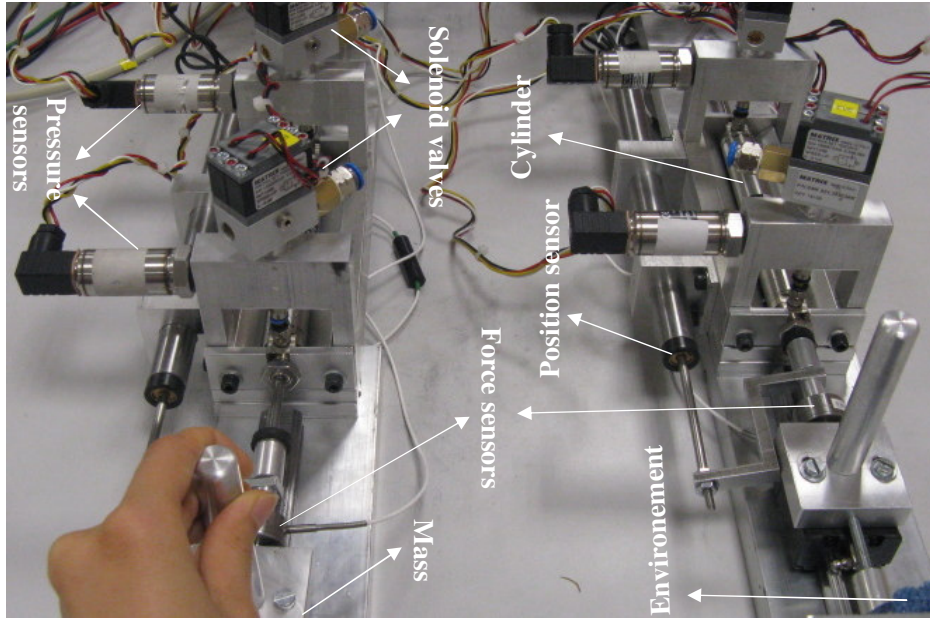


Fig. 5. Pneumatic master-slave teleoperation experimental setup

In this study, the master and the slave's valves/actuator are considered to be similar. However, the proposed sliding mode controller provides robust performance despite model uncertainties and variations. First, the stability condition (13) based on the Lyapunov candidate function is always met even when the parameters in Tab. II are not the same for the master and the slave robots. Second, in practice, the valves and actuators used in the master and slave are not exactly the same due to imprecision of manufacturing of electronic and mechanic components. The above points are further evidence of the robustness of our controller. For teleoperation with different kinematics and drive actuations for the master and slave manipulators (e.g., in micro-macro system), the reader can refer to (Lee and Li, 2005).

For the PEB and DFR systems, the sliding surface of the position-controlled slave is normalized as

$$s = \frac{\ddot{e}}{\omega^2} + 2\frac{\xi}{\omega}\dot{e} + e \quad (38)$$

This is because, in practice, it is easier if the sliding surface for position control is chosen in order to have the same dimension as positions as in (38) and not accelerations as in (11). The first derivative of the position error in (38) is computed through a backward difference method applied on the position signal followed by a de-noising second-order Butterworth filter with a cutoff frequency of 70Hz. The second derivative is computed in the same way from the filtered

first-derivative signal. The filter bandwidth was chosen to be large enough (70 Hz) with respect to the bandwidth of the human hand movement, i.e. the input's bandwidth of the system. According to (Shimoga, 1993), the maximum bandwidth with which the human finger normally reacts to a tactile input is about 8 - 10 Hz. As a result, most of information in position, velocity and acceleration signals is conserved. Only high frequency oscillations and vibrations are attenuated when using such a filter.

There exist several strategies to estimate the velocity and acceleration from the position information. Backward difference method, which is considered to be the simplest numerical method for differentiating a signal, is used in our application for an easier experimental implementation. The differentiator is sampled at 500 Hz and associated to the de-noising Butterworth low-pass filter (i.e. defined previously). However, the use of low-pass filters to compute the velocity and acceleration can introduce additional phase shift that somewhat limits the closed-loop performance. As a result, alternative solutions for differentiation of signals with noise attenuation that do not introduce significant delays have been proposed in the literature. The aim of these methods is to realize filters that approximate the ideal differentiator in a certain range of frequencies. Assuming that the position can be approximated with a low-order polynomial, a differentiator based on the Newton predictor was proposed in (Ovaska and Vainio, 1992). Differentiators based on FIR or IIR filters have been presented in (Vainio et al., 1997); these approaches are normally called predictive post-filtering. Another method for the velocity estimation relies on the state observer theory. Knowing the plant model, estimators based on Kalman filter (Belanger, 1992; Jaritz and Spong, 1996), Nicosia observer (Nicosia and Tomei, 1990), and Luenberger observers and nonlinear observers (Bodson et al., 1995; Yang and Ke, 2000) have been investigated. Also, (Janabi-Sharifi et al., 2000) present methods for the velocity estimation from discrete and quantized position samples using adaptive windowing. Other solutions based on the sliding mode observers were presented in (Levent, 1998; Sidhom et al., 2010).

There is a trade-off between tracking error and chattering to achieve good performances. In theory, the characteristics of the control system is determined by the poles of the second-order reference model (38), which depends on the parameters  $\omega$  and  $\zeta$ . It is noteworthy that when  $\zeta$  and  $\omega^2$  in (38) increase, the averaged tracking error is better but the chattering increases. It means that the response is around the reference in the transient and steady state but more oscillations can be observed due to the noise of velocity's and acceleration's estimations. This is understandable from the perspective of moving the poles of a second-order transfer function farther to the left of the imaginary axis – faster pole locations result in faster convergence of the tracking error to zero. Since  $\zeta/\omega$  is multiplied by  $\dot{e}$  in the sliding surface (38), the noise in  $\dot{e}$  (corresponding to undesired oscillations and vibrations) will be amplified with a small value of  $\zeta/\omega$ ,

resulting in increased chattering problem. Similarly, when  $1/\omega^2$  is small, the contribution of the noise present in  $\ddot{e}$  is amplified in (38). To efficiently damp the oscillations and vibrations in  $\ddot{e}$ , which suffers from differentiation noise,  $\omega$  is generally not chosen to be too high in practice. For a good trade-off between the position tracking performance and the chattering problem, the parameters  $\zeta = 0.5$  and  $\omega = 70$  rad/s will be used in our experiment.

Since the coefficient of  $e$  in (38) equals 1, in the steady state we will have  $s = e$ . We define the tolerable range (or “threshold”) of this error as a neighbourhood of radius  $\varepsilon_p$ . In the experiments,  $\varepsilon_p$  is chosen equal to 0.5 mm in order to guarantee good position tracking performance without causing too much switching of the valves. Concerning the force controller, a force error threshold  $\varepsilon_f$  needs to be chosen. In practice, we choose  $\varepsilon_f$  equal to 0.1 N to achieve good force tracking responses. With the ideal position and force tracking errors chosen as 0.5 mm and 0.1 N, respectively, high transparency is obtained in the pneumatic actuated teleoperation system with inexpensive on/off valves.

To resume, the following table presents all physical parameters used in the paper.

TABLE II: MODEL AND CONTROLLER PARAMETERS

Parameter	Value	Unit	Description
$P_{atm}$	$10^5$	Pa	Atmosphere pressure
$P_{sa}$	$3.10^5$	Pa	Supply pressure
$r$	287	J/kg/K	Perfect gas constant
$T_a$	293.15	K	Supply temperature
$C_r$	0.433		Critical pressure ratio
$\alpha$	1.2		Polytropic constant
$l$	0.1	m	Cylinder stroke
$S_p$	$182 \cdot 10^{-6}$	m <sup>2</sup>	Piston area of chamber p
$S_n$	$182 \cdot 10^{-6}$	m <sup>2</sup>	Piston area of chamber n
$M$	1	kg	Moving load
$b$	20	N.s/m	Viscosity coefficient
$T_{op}$	1.3	ms	Opening time of solenoid valve
$T_{cl}$	0.2	ms	Closing time of solenoid valve
$T$	2	ms	Sampling time of controller
$f_c$	70	Hz	Cut-off frequency of filter
$\omega$	70	rad/s	Angular frequency
$\zeta$	0.5		Damping coefficient
$\varepsilon_p$	0.5	mm	Position threshold
$\varepsilon_f$	0.1	N	Force threshold

## 4.2. Experimental Results

### 4.2.1. Time Analysis

Figure 6 shows the master and the slave force and position tracking profiles in free space and in contact motion for the PEB teleoperation system. Figures 7 and 8 illustrate the same profiles for the FEB and the DFR systems, respectively.

In the experiments, for the first few seconds, the master is moved back and forth by the user when the slave is in free space. The small but nonzero values for  $F_e$  when the slave is in free space are due to the mass of the handle-like connector between the slave's force sensor and the slave's end-effector (tip). Similarly, the small but nonzero values for  $F_h$  during slave's free motion are due to the mass of the master's handle, which lies between the force sensor and the operator's hand. Note that the fast movements of the master in the first few seconds do not represent oscillations; rather, they are intentionally created by the operator to examine the system stability and performance in free motion.

Next, the slave makes contact with a hard environment, i.e., a sponge with rigid structure. The operator pushes against the master handle leading to different levels of the slave/environment contact forces. The fact that the position profiles remain constant during the contact mode is simply because under hard contact the slave cannot penetrate the environment regardless of the operator's force.

As it can be observed in Fig. 6 to Fig. 8, limited amounts of vibration in the force and position responses are introduced by the discrete operation of the on/off solenoid valves. These vibrations increase under hard contact for the force profiles due to higher valve switching activities but are otherwise negligible. Another effect caused by the on/off solenoid valves, which cannot be seen in the above figures, is the acoustic noise. Indeed, as a solenoid valve switches between the two operating positions (open or closed), a clicking sound is generated.

As illustrated in Fig. 6, the PEB system provides a good position tracking responses. It can be seen that the slave rapidly tracks the master's movement in free space and also in contact mode. However, the force response is not as good because no force sensor is used. On the other hand, the force tracking performance of the FEB system is much better, thanks to the knowledge of the force information. Nonetheless, the position tracking deteriorates in FEB control – as it can be seen in Fig. 7, the slave's movement does not accurately track the master's movement. Fig. 6 and Fig. 7 show the tradeoffs between position tracking and force tracking as long as only either both positions or both forces are available for feedback (i.e., PEB and FEB control, respectively).

Interestingly, the DFR system in Fig. 8 provides an improvement in terms of position tracking response compared to

the FEB system. It also displays a superior force tracking performance compared to the PEB, especially under contact motion. However, a drawback of the DFR system is that higher oscillations and vibrations are present in the force and position responses under contact motion. Consequently, when operator's force level increases, the DFR system is less stable than the other cases. This result agrees with the previous theoretical work but is shown for the first time for on/off valve actuated pneumatic teleoperation systems.

It is noteworthy that the magnitude of the hand-master interaction force in the following Figures (Figs. 6, 7, and 8) is higher than expected during free motion. This behavior is due to frictions induced by our rail-guide system, which uses floating balls between the carriage and the rail profile. This component introduces friction during the displacement of the robot. However, during the contact phases, the friction has a negligible influence since the pneumatic actuators move little.

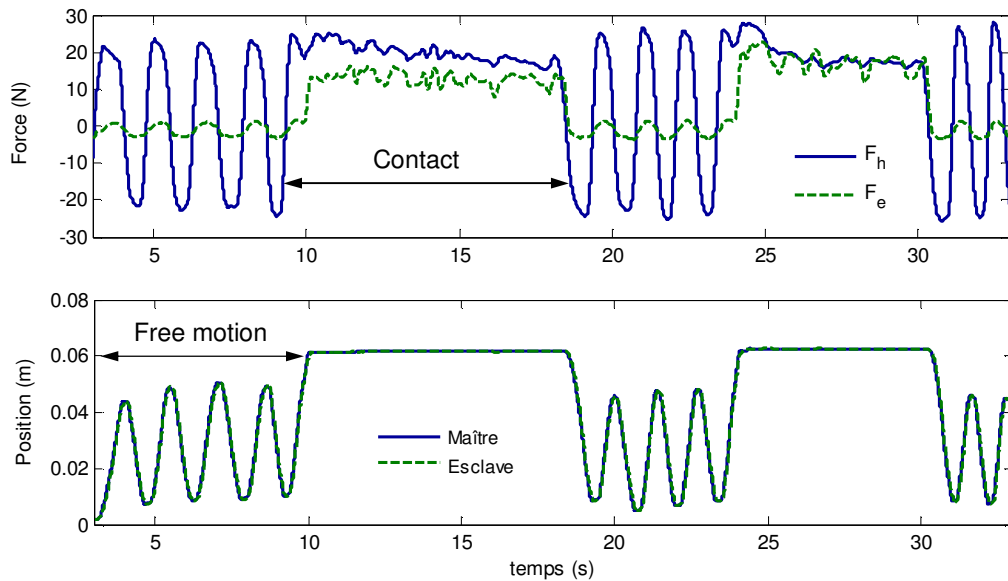


Fig. 6. Position and force responses of the PEB system

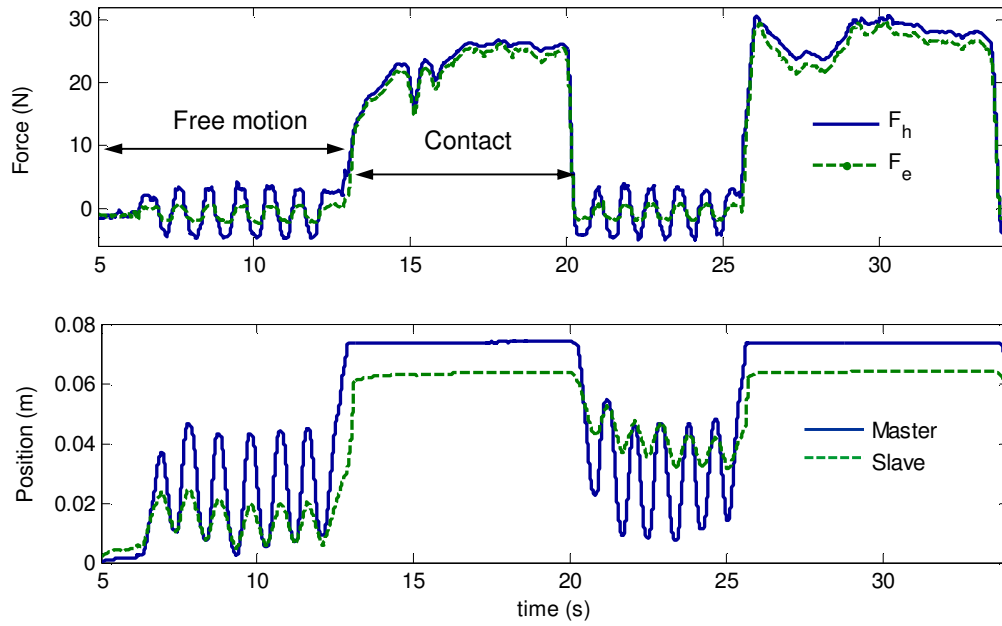


Fig. 7. Position and force responses of the FEB system

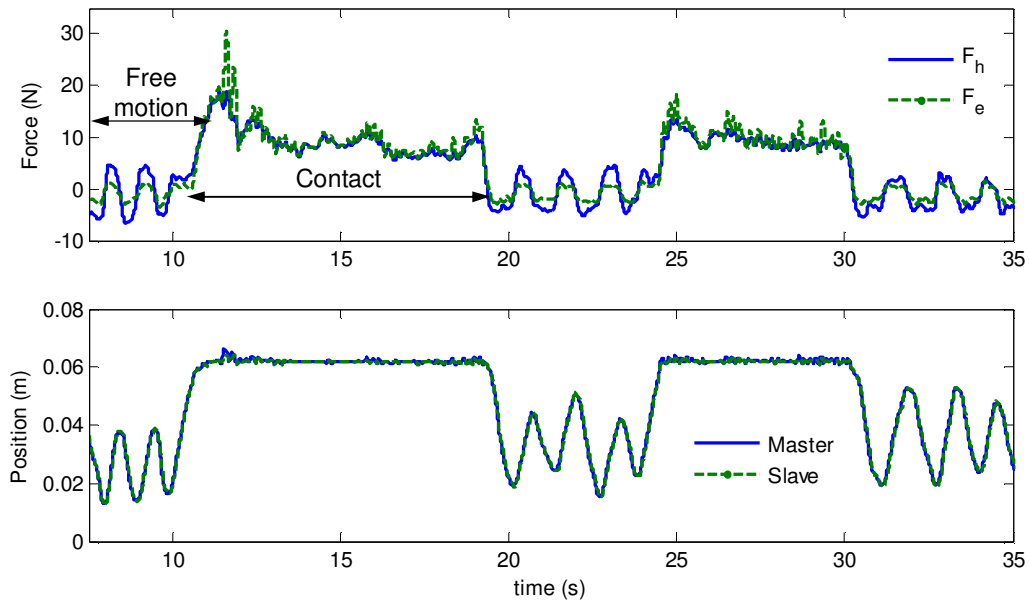


Fig. 8. Position and force responses of the DFR system

Among the three architectures, the DFR scheme seems to be a better choice to obtain a good transparency. Although the various teleoperation controllers have previously been compared from a performance perspective in the literature (Lau and Wai, 2005; Tavakoli et al., 2007), this is the first study to show that it is possible to achieve stability and satisfactory performance using manipulators actuated by low-cost switching on/off valves.

#### 4.2.2. Frequency Analysis

In the following, we use another experimental method for assessing system transparency that approximates the system with an LTI model. If this assumption cannot be made for the nonlinear model of pneumatic actuators, the time-domain profiles of Figs. 6–8 sufficiently evaluate transparency.

For the frequency analysis of the approximate LTI model, we use the classical hybrid representation of the two-port network model of a master-slave system. A complete discussion of the hybrid matrix analysis can be found in (Lawrence, 1992; Salcudean et al., 2000). In this representation,

$$\begin{bmatrix} F_h \\ -Y_s \end{bmatrix} = \begin{bmatrix} h_{11} & h_{12} \\ h_{21} & h_{22} \end{bmatrix} \begin{bmatrix} Y_m \\ F_e \end{bmatrix} \quad (39)$$

In an ideally transparent teleoperation system, the master and the slave positions and forces will match regardless of the operator and environment dynamics:

$$Y_m = Y_s \quad , \quad F_h = F_e \quad (40)$$

From (39) and (40), perfect transparency is achieved if and only if the hybrid matrix  $H$  has the following form:

$$H_{\text{ideal}} = \begin{bmatrix} 0 & 1 \\ -1 & 0 \end{bmatrix} \quad (41)$$

Thus, by finding the hybrid matrix of our experimental pneumatic teleoperation system through system identification tests and comparing to the above ideal hybrid matrix, the transparency of the system can be evaluated.

Each element of the  $H$  matrix has a physical meaning. The hybrid parameter  $h_{11} = F_h/Y_m|_{F_e=0}$  is the input impedance in free-motion condition. The parameter  $h_{12} = F_h/F_e|_{Y_m=0}$  is a measure of force tracking when the master is locked in motion (perfect force tracking when  $h_{12} = 1$ ). The parameter  $h_{21} = -Y_s/Y_m|_{F_e=0}$  is a measure of position tracking performance when the slave is in free space (perfect position tracking when  $h_{21} = -1$ ). The parameter  $h_{22} = -Y_s/F_e|_{Y_m=0}$  is the output admittance when the master is locked in motion. Nonzero values for  $h_{22}$  indicate that even when the master is locked in place, the slave will move in response to slave/environment contacts.

Since  $F_e = 0$  in the free-motion tests, the frequency responses  $h_{11} = F_h/Y_m|_{F_e=0}$  and  $h_{21} = -Y_s/Y_m|_{F_e=0}$  can be found by applying the spectral analysis function *spa* of Matlab. Also, by using contact-mode test data, the other two hybrid parameters can be obtained as  $h_{12} = F_h/F_e - h_{11} Y_m/F_e$  and  $h_{22} = -Y_s/F_e - h_{21} Y_m/F_e$  (Tavakoli et al., 2008).

The magnitude of the hybrid parameters of the PEB, FEB and DFR teleoperation systems is shown in Fig. 9. As it can be seen,  $|h_{12}|$  and  $|h_{21}|$  in the DFR scheme are close to 0 dB, reflecting excellent transparency in terms of force and position tracking for frequencies up to 100 rad/s. With regard to the PEB scheme, closeness to 0 dB of  $|h_{21}|$  indicates that the system ensures good position tracking in free space. On the other hand, the degradation of  $|h_{12}|$  spectra under PEB is in agreement with the time-domain force profiles in Figs. 6–8, where force tracking in the PEB case is not on par with that in the other cases. Contrary to the PEB system, the FEB system only guarantees good transparency in terms of force tracking but not position tracking, as illustrated in the  $|h_{12}|$  and  $|h_{21}|$  parameters of Fig. 9.

Relatively high values of  $h_{11}$  for the PEB scheme are an evidence of the fact that even when the slave is in free space, the user will feel residual forces that depend on the position tracking error of the master and the slave robots. Concerning the DFR and FEB schemes, thanks to the measurements of  $f_e$ , their input impedances in free-motion condition ( $h_{11}$ ) will be lower, which makes the feeling of free space much more realistic (Tavakoli et al., 2007). Lastly, consistent with (41), low values of the output admittance ( $h_{22}$ ) in the three architectures show that the slave’s movement in response to external force disturbances quickly converges to zero when the master is locked in motion.

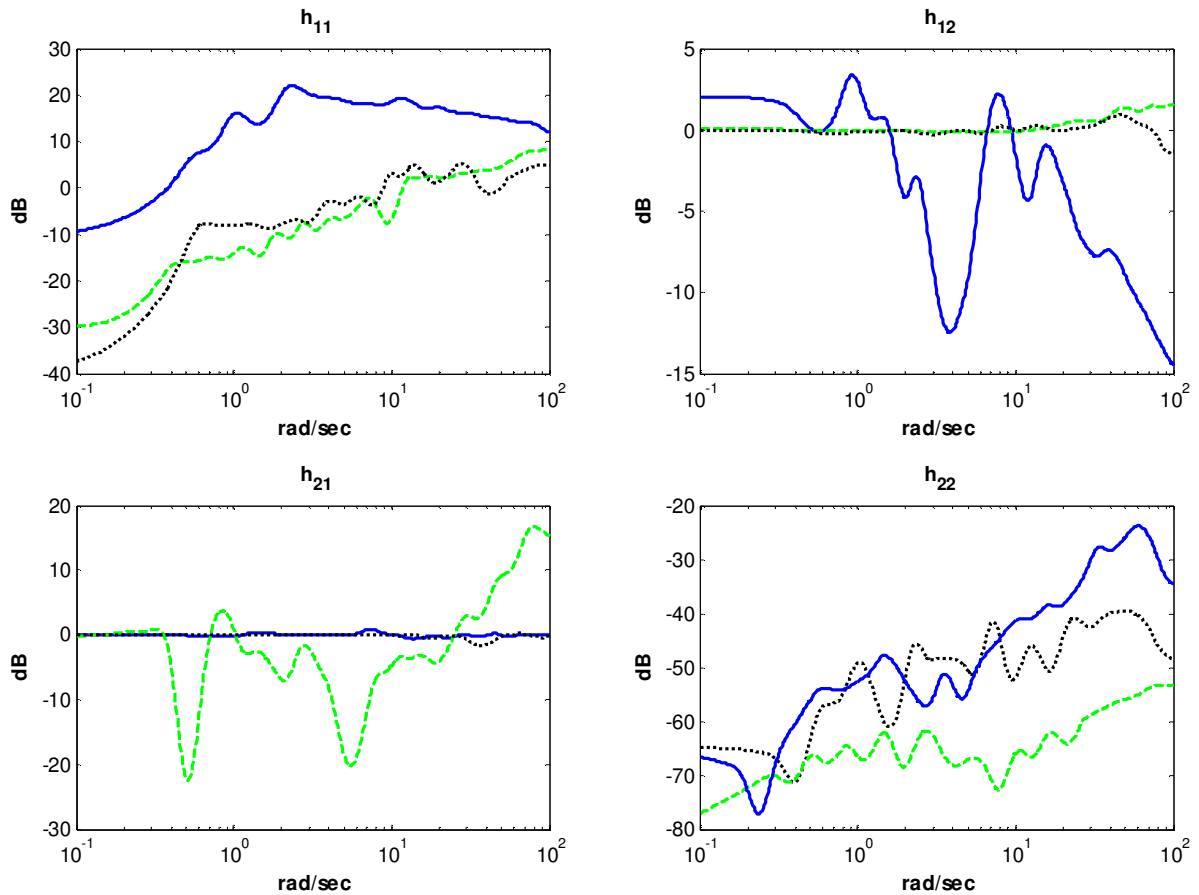


Fig. 9. Frequency spectra of the hybrid parameters under sliding control: PEB (Solid), FEB (Dashed), DFR (Dotted)

## 5. Extension to a five-mode Control Scheme

### 5.1. Principle

In this section, we investigate the use of a sliding control with five switching modes (see Table III) instead of the three standard modes presented in section 3. The new system has two extra modes, which are defined by connecting only one chamber to the supply while leaving the other chamber locked.

TABLE III: FIVE POSSIBLE CONTROL MODES

	Mode 1	Mode 2	Mode 3	Mode 4	Mode 5
Chamber p	fills	exhausts	closed	fills	closed
Chamber n	exhausts	fills	closed	closed	fills
Control $u$	1	-1	0	0.5	-0.5
$\underline{U} = [U_1 \ U_2 \ U_3 \ U_4]$	[1 0 1 0]	[0 1 0 1]	[0 0 0 0]	[1 0 0 0]	[0 0 0 1]

As it can be seen in Table III, the first three modes in the 5MCS are inherited from the 3MCS. Modes 4 and 5 are added in the 5MCS in order to offer more possibilities in terms of switching choices and improve the behavior of the system by reducing switching activity of the valves. Similar to mode 1, mode 4 allows moving the cylinder rod in the same direction but with a slower dynamics (because in mode 4 the chamber n is closed as opposed to exhausting as in mode 1). Mode 4 may be considered as an intermediate mode (or average) between modes 1 and 3, where the control vector  $u$  is chosen equal to 0.5 (Table III). On the other hand, mode 5 whose control vector  $u$  equals  $-0.5$  is used to move the cylinder rod in the other direction and could be regarded as an intermediate option between modes 2 and 3.

The operation of the 5-mode sliding controller is based on the following three principles:

1. When  $|s|$  is within the interval  $[0, \varepsilon]$ , mode 3 ( $u = 0$ ) is used to conserve energy and reduce chattering.
2. To be able to switch between modes 1 and 4 or modes 2 and 5, a threshold  $\varepsilon_1$  is introduced where  $\varepsilon_1 > \varepsilon$ . When  $|s|$  is within the interval  $(\varepsilon, \varepsilon_1)$ , either mode 4 or mode 5 ( $u = \pm 0.5$ ) is used to provide slower dynamics compared to modes 1 or 2 ( $u = \pm 1$ ), respectively. Still, the piston is actuated to move in the direction that minimizes  $s$ .
3. When  $|s|$  is within the interval  $[\varepsilon_1, \infty[$ , either mode 1 or mode 2 ( $u = \pm 1$ ) is used to provide fast dynamics, highly accelerating the piston in the direction that minimizes  $s$ .

A presentation of the 5-mode controller diagram can be shown in Fig. 10.

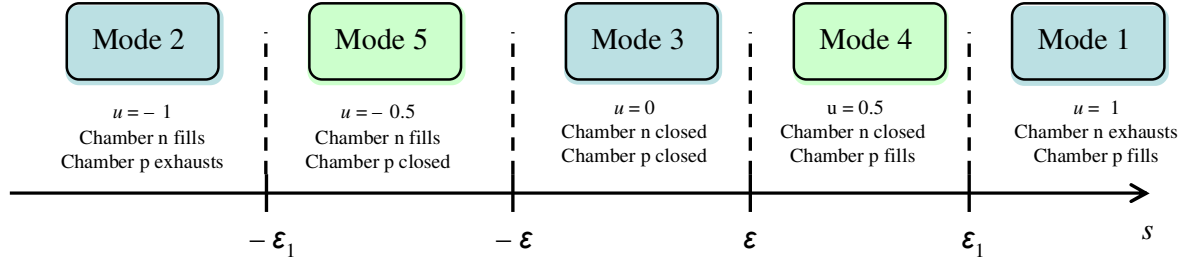


Fig. 10. 5-mode controller diagram

In summary, the new control law for the 5MCS can be given as

$$u = \begin{cases} +/\text{-} \text{sign}(s) & \text{if } |s| \geq \varepsilon_1 \\ +/\text{-} 0.5 \text{sign}(s) & \text{if } \varepsilon < |s| < \varepsilon_1 \\ 0 & \text{if } |s| \leq \varepsilon \end{cases} \quad (42)$$

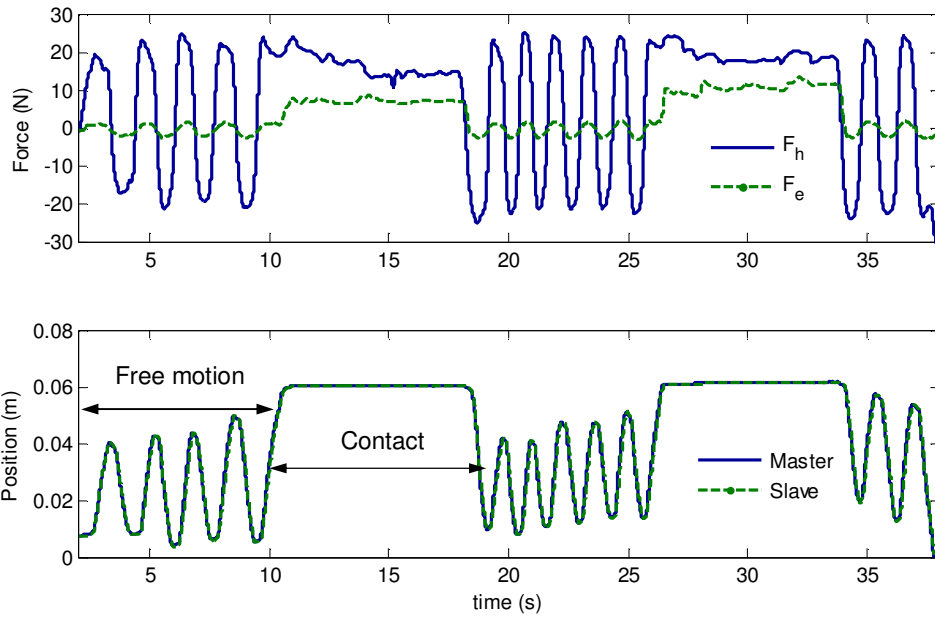
As it can be seen later in experiment, the 5MCS offers an advantage in terms of valves switching activities over the 3MCS. However, the addition of a new threshold (i.e.,  $\varepsilon_1$ ) can make the tuning more complex in the 5MCS. Similar to  $\varepsilon$ ,  $\varepsilon_1$  is chosen based on the trade-off between accuracy and chattering. If  $\varepsilon_1$  is very small (i.e.,  $\varepsilon_1 \rightarrow \varepsilon$ ), the dynamic behavior of the 5MCS becomes similar to the 3MCS. In this case the two additional modes will not offer additional benefits and chattering will not be improved. On the other hand, a modest value of  $\varepsilon_1$  allows to reduce the switching activity of the valves and maintain the tracking properties of the systems.”

## 5.2. Comparison between the 5MCS and the 3MCS

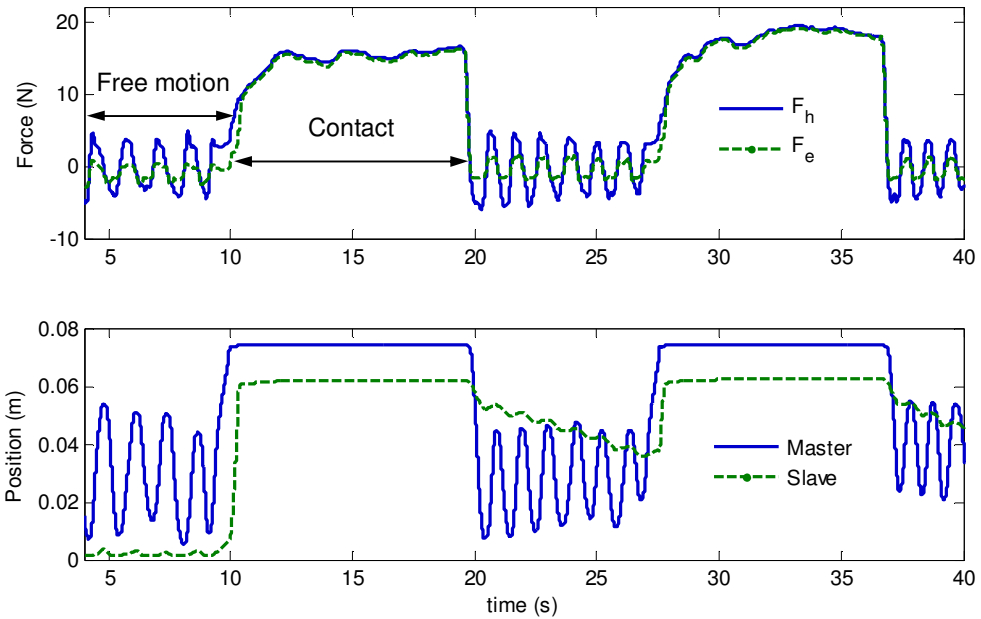
To facilitate a comparison of the 5MCS and 3MCS performances, all controller parameters are chosen to be similar for both cases, i.e.,  $\zeta = 0.5$ ,  $\omega = 70$  rad/s,  $\varepsilon_p = 0.5$  mm for the position controller, and  $\varepsilon_f = 0.1$  N for the force controller. In addition, for the 5MCS, two more parameters need to be adjusted (i.e., a position threshold  $\varepsilon_{1p}$  and a force threshold  $\varepsilon_{1f}$ ). Their values found by experimental trials are 1 mm and 0.5 N, respectively.

Fig. 11 shows the master and the slave force and position tracking profiles in the 5MCS teleoperation system. In the PEB and FEB systems, the transparency under 5MCS seems to be similar with that under the 3MCS (compared with Fig. 6 – Fig. 7). On the other hand, under DFR control, less oscillation is observed in the 5MCS case than in the 3MCS case. This allows to achieve higher contact force quality, improving the operator’s perception.

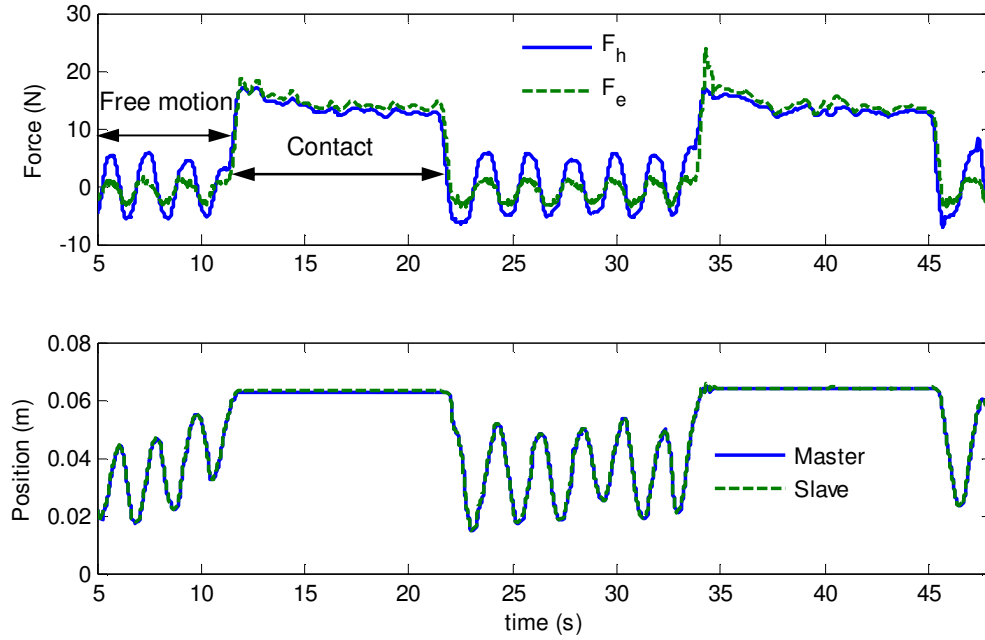
As previously explained, the high values of free-motion force readings are due to the friction in our rail-guide system.



(a). PEB architecture



(b). FEB architecture



(c). DFR architecture

Fig. 11. Transparency of the teleoperation system with 5MCS

To show further benefits of the 5MCS teleoperation, we can take the transparency analysis beyond only studying the force and position responses. Note that the major drawback of solenoid valves is that they tend to switch a lot which both creates noise and non-smooth tracking behavior. Any improvement in this regard is highly important. We will show in the following that the 5MCS teleoperation results in reduced switching activities of the on/off valves while maintaining position and force tracking responses. To do this, a frequency analysis of the control signals (controller outputs) is carried out. For each of the master and slave manipulators there exist four control signals ( $U_1$ ,  $U_2$ ,  $U_3$  and  $U_4$ ), thus eight signals for the overall system. In the following, due to the space restrictions, we only compare the spectra of  $U_1$  of the master side. Similar results can be observed for the other control signals. The frequency responses can be found by using the discrete fast Fourier transform *fft* command in Matlab. The spectral analysis of the control signal  $U_1$  obtained with the 5MCS and 3MCS are shown in Fig. 12.

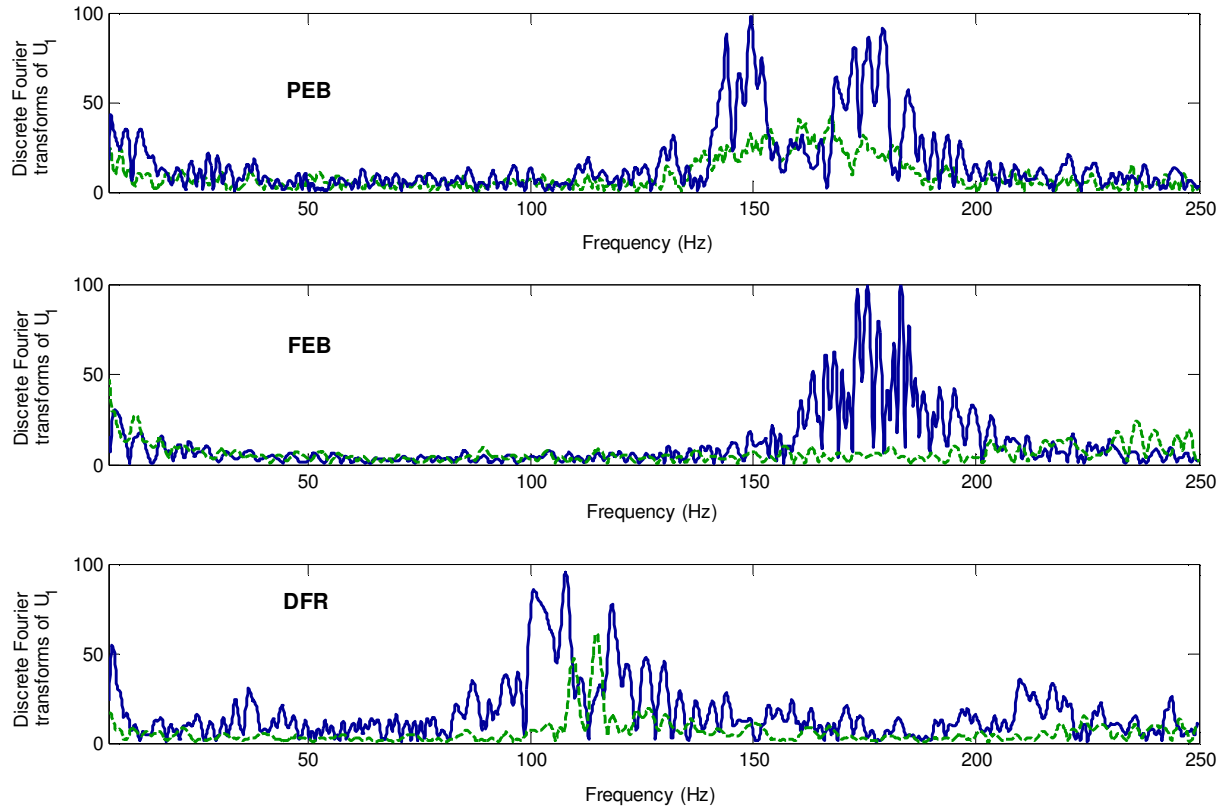


Fig. 12. Discrete Fourier transforms of the control signal  $U_1$  for the master manipulator: 3MCS (Solid), 5MCS (Dashed)

As it can be observed, for all three architectures (PEB, FEB, and DFR), the magnitude  $|U_1|$  of the spectra is lower in the 5MCS case than in the 3MCS case over almost all frequencies, and especially so at high frequencies. This shows that by using two additional modes, the on/off activity of the valves has been reduced, which allows to provide better tracking responses with smoother dynamics and less oscillations, particularly over high frequencies.

Based on these results, it is clear that the 5MCS is an interesting alternative to save energy and improve the valve's lifetime at no cost to teleoperation transparency. An area of possible future development is methods for adjusting the parameters  $\varepsilon_{1p}$  and  $\varepsilon_{1f}$  for best performance.

## 6. Conclusions

In this paper, pneumatic actuators with inexpensive solenoid valves are chosen for the development of a master-slave teleoperation system – such pneumatic-actuated teleoperation systems can have wide uses such as in-MRI robot-assisted intervention. To efficiently switch the on/off valves for transparent haptic teleoperation, sliding mode controllers are proposed and implemented in a real-world test bed. In order to evaluate the efficacy of the sliding mode approach, a

comparison of the transparency and stability has been investigated between three control architectures (position-error-based, force-error-based, and direct-force-reflection) in a two-channel bilateral teleoperation system. The drawbacks of the PEB and FEB schemes in terms of less-than-ideal force or position tracking performance are analytically and experimentally demonstrated. Also, the DFR control scheme is shown to be highly transparent as both force and position sensors are used.

In order to improve the dynamic performance and reduce the chattering problem in solenoid valve actuated pneumatic teleoperation systems, a five-mode sliding control scheme has been investigated, which can be considered as an extension to the three-mode sliding controller. Our study demonstrated that by increasing the number of the control actions possible for the valves, we can reduce the valves' switching activities, hence improving the valve life times at no cost to teleoperation transparency.

An area of future work, especially when the number of switching modes increases, is to efficiently tune the threshold parameters  $\varepsilon$  and  $\varepsilon_1$  for best tradeoff between tracking accuracy and chattering. Another aspect of our future work is to implement the proposed sliding bilateral control on a direct-drive, multi-DOF teleoperation system.

## References

- Aliaga, I., Rubio, A., Sanchez, E., 2004. Experimental quantitative comparison of different control architectures for master-slave teleoperation. *IEEE Transactions on Control Systems Technology* 12, 2–11.
- Anderson, R.J., Spong, M.W., 1989. Bilateral control of teleoperators with time delay. *IEEE Transactions on Automatic Control* 34, 494–501.
- Arcara, P., Melchiorri, C., 2002. Control schemes for teleoperation with time delay: A comparative study. *Robotics and Autonomous Systems* 38, 49–64.
- Aziminejad, A., Tavakoli, M., Patel, R.V., Moallem, M., 2008. Stability and performance in delayed bilateral teleoperation: Theory and experiments. *Control Engineering Practice* 16, 1329–1343.
- Belanger, P.R., 1992. Estimation of angular velocity and acceleration from shaft encoder measurements, *IEEE International Conference on Robotics and Automation*. pp. 585–592.
- Ben-Dov, D., Salcudean, S., 1993. A force-controlled pneumatic actuator for use in teleoperation masters, *IEEE International Conference on Robotics and Automation*. pp. 938–943.
- Blackburn, R., 1960. *Shearer, Fluid Power Control*. John Wiley and Sons, Inc.
- Bodson, M., Chiasson, J., Novotnak, R.T., 1995. Nonlinear speed observer for high-performance induction motor control. *IEEE Transactions on Industrial Electronics* 42, 337–343.
- Chopra, N., Berestesky, P., Spong, M.W., 2008. Bilateral Teleoperation Over Unreliable Communication Networks. *Control Systems Technology, IEEE Transactions on* 16, 304–313.
- Durbha, V., Li, P.Y., 2009. Passive bilateral tele-operation and human power amplification with pneumatic actuators. *Proceedings of ASME Dynamic Systems and Control Conference, California, USA* 1–8.
- Fite, K.B., Speich, J.E., Goldfarb, M., 2001. Transparency and stability robustness in two-channel bilateral telemanipulation. *Journal of Dynamic Systems, Measurement, and Control* 123, 400–407.
- Guerriero, B., Book, W., 2008. Haptic Feedback Applied to Pneumatic Walking. *ASME Conf. Proc.* 591–597.
- Hashtrudi-Zaad, K., Salcudean, S.E., 2001. Analysis of control architectures for teleoperation systems with impedance/admittance master and slave manipulators. *The International Journal of Robotics Research* 20, 419.
- Hodgson, S., Le, M.Q., Tavakoli, M., Pham, M.T., 2011. Improved Tracking and Switching Performance in Position-Controlled Nonlinear Pneumatic-Actuated Robots. *Mechatronics*, to be published.
- Hokayem, P.F., Spong, M.W., 2006. Bilateral teleoperation: An historical survey. *Automatica* 42, 2035–2057.
- Itoh, T., Kosuge, K., Fukuda, T., 2000. Human-machine cooperative telemanipulation with motion and force scaling using task-oriented virtual tool dynamics. *IEEE Transactions on Robotics and Automation* 16, 505–516.

- Janabi-Sharifi, F., Hayward, V., Chen, C.S.J., 2000. Discrete-time adaptive windowing for velocity estimation. *IEEE Transactions on Control Systems Technology* 8, 1003–1009.
- Jaritz, A., Spong, M.W., 1996. An experimental comparison of robust control algorithms on a direct drive manipulator. *IEEE Transactions on Control Systems Technology* 4, 627–640.
- Kim, J., Chang, P.H., Park, H.S., 2005. Transparent teleoperation using two-channel control architectures. *IEEE/RSJ International Conference on Intelligent Robots and Systems (IROS) 1953–1960*.
- Lau, H.Y.K., Wai, L.C.C., 2005. Implementation of position-force and position-position teleoperator controllers with cable-driven mechanisms. *Robotics and Computer-Integrated Manufacturing* 21, 145–152.
- Lawrence, D.A., 1992. Designing teleoperator architectures for transparency. *IEEE International Conference on Robotics and Automation (ICRA), France 1406–1411*.
- Lawrence, D.A., 1993. Stability and transparency in bilateral teleoperation. *IEEE Transactions on Robotics and Automation* 9, 624–637.
- Le, M.Q., Pham, M.T., Moreau, R., Simon, J.P., Redarce, T., 2011. Force Tracking of Pneumatic Servo Systems using on/off Solenoid Valves based on a Greedy Control Scheme. *ASME Journal of Dynamic Systems, Measurement, and Control* 133.
- Lee, D., Li, P.Y., 2003. Passive bilateral feedforward control of linear dynamically similar teleoperated manipulators. *IEEE Transactions on Robotics and Automation* 19, 443–456.
- Lee, D., Li, P.Y., 2005. Passive bilateral control and tool dynamics rendering for nonlinear mechanical teleoperators. *Robotics, IEEE Transactions on* 21, 936–951.
- Levent, A., 1998. Robust exact differentiation via sliding mode technique. *Automatica* 34, 379–384.
- Maurette, M., Boissier, L., Delpech, M., Proy, C., Quere, C., 1997. Autonomy and remote control experiment for lunar rover missions. *Control Engineering Practice* 5, 851–857.
- McCloy, D., 1968. Discharge characteristics of servo valve orifices. *Fluid International Conference* 43–50.
- Nguyen, T., Leavitt, J., Jabbari, F., Bobrow, J.E., 2007. Accurate sliding-mode control of pneumatic systems using low-cost solenoid valves. *IEEE/ASME Transactions on mechatronics* 12, 216–219.
- Nicosia, S., Tomei, P., 1990. Robot control by using only joint position measurements. *IEEE Transactions on Automatic Control* 35, 1058–1061.
- Niemeyer, G., Slotine, J.J., 1991. Stable adaptive teleoperation. *IEEE Journal of oceanic engineering* 16, 152–162.
- Ningbo Yu, Hollnagel, C., Blickenstorfer, A., Kollias, S.S., Riener, R., 2008. Comparison of MRI-Compatible Mechatronic Systems with Hydrodynamic and Pneumatic Actuation. *IEEE/ASME Transactions on Mechatronics* 13, 268–277.
- Norisugu, T., 1985. Pulse-width modulated feedback force control of a pneumatically powered robot hand. *Proceedings of International Symposium of Fluid Control and Measurement* 47–52.
- Oboe, R., Fiorini, P., 1998. A Design and Control Environment for Internet-Based Telerobotics. *International Journal of Robotics Research* 17, 433–449.
- Ovaska, S.J., Vainio, O., 1992. Recursive linear smoothed Newton predictors for polynomial extrapolation. *IEEE Transactions on Instrumentation and Measurement* 41, 510–516.
- Ross, S., Waliany, R., Swanson, M., 2009. Inverse Kinematics and Balance Control for Intuitive Teleoperation of a Six-Legged Mining Robot.
- Sabater, J.M., Saltarén, R.J., Aracil, R., Yime, E., Azorín, J.M., 2006. Teleoperated parallel climbing robots in nuclear installations. *Industrial Robot: An International Journal* 33, 381–386.
- Salcudean, S.E., Wong, N.M., Hollis, R.L., 1995. Design and control of a force-reflecting teleoperation system with magnetically levitated master and wrist. *IEEE Transactions on Robotics and Automation* 11, 844–858.
- Salcudean, S.E., Zhu, M., Zhu, W.-H., Hashtrudi-Zaad, K., 2000. Transparent Bilateral Teleoperation under Position and Rate Control. *International Journal of Robotics Research* 19, 1185–1202.
- Sanchez, L.A., Le, M.Q., Liu, C., Zemiti, N., Poignet, P., 2012. The Impact of Interaction Model on Stability and Transparency in Bilateral teleoperation for Medical Applications. *IEEE International Conference on Robotics and Automation (ICRA)*, to be published.
- Sheridan, T.B., 1995. Teleoperation, telerobotics and telepresence: A progress report. *Control Engineering Practice* 3, 205–214.
- Shih, M.C., Ma, M., 1998. Position control of a pneumatic rodless cylinder using fuzzy PWM control method. *Mechatronics* 41, 241–253.
- Shimoga, K.B., 1993. A survey of perceptual feedback issues in dexterous telemanipulation: Part I. Finger force feedback. *Proceedings in IEEE Virtual Reality Annual International Symposium* 263–270.
- Sidhom, L., Pham, M.T., Thevenoux, F., Gautier, M., 2010. Identification of a robot manipulator based on an adaptive higher order sliding modes differentiator. *IEEE/ASME International Conference on Advanced Intelligent Mechatronics* 1093–1098.
- Slotine, J.J., Li, W., others, 1991. *Applied nonlinear control*. Prentice Hall Englewood Cliffs, NJ.
- Stassen, H.G., Smets, G.J.F., 1997. Telemanipulation and telepresence. *Control Engineering Practice* 5, 363–374.
- Stramigioli, S., van der Schaft, A., Maschke, B., Melchiorri, C., 2002. Geometric scattering in robotic telemanipulation. *IEEE Transactions on Robotics and Automation* 18, 588–596.
- Tadano, K., Kawashima, K., 2007. Development of a master slave system with force sensing using pneumatic servo system for laparoscopic surgery. *IEEE International Conference on Robotics and Automation*, 1 18, 947–952.
- Taghizadeh, M., Ghaffari, A., Najafi, F., 2009. Improving dynamic performances of PWM-driven servo-pneumatic systems via a novel pneumatic circuit. *ISA Transactions* 48, 512–518.
- Tavakoli, M., Aziminejad, A., Patel, R.V., Moallem, M., 2007. High-fidelity bilateral teleoperation systems and the effect of multimodal haptics.

- IEEE Transactions on Systems, Man, and Cybernetics, Part B 37, 1512–1528.
- Tavakoli, M., Patel, R.V., Moallem, M., 2008. Haptics for Teleoperated Surgical Robotic Systems. World Scientific.
- Tondu, B., Ippolito, S., Guiochet, J., Daidie, A., 2005. A Seven-degrees-of-freedom Robot-arm Driven by Pneumatic Artificial Muscles for Humanoid Robots. *The International Journal of Robotics Research* 24, 257–274.
- Utkin, V., Chang, H.C., 2002. Sliding mode control on electro-mechanical systems. *Mathematical Problems in Engineering* 8, 451–473.
- Vainio, O., Renfors, M., Saramaki, T., 1997. Recursive implementation of FIR differentiators with optimum noise attenuation. *IEEE Transactions on Instrumentation and Measurement* 46, 1202–1207.
- Yang, S.M., Ke, S.J., 2000. Performance evaluation of a velocity observer for accurate velocity estimation of servo motor drives. *IEEE Transactions on Industry Applications* 36, 98–104.
- Yoshikawa, T., Ichino, Y., 2003. Impedance identification of human fingers using virtual task environment. *IEEE/ASME International Conference on Advanced Intelligent Mechatronics (AIM)* 2, 759–764.
- Zhu, M., Salcudean, S.E., 1995. Achieving transparency for teleoperator systems under position and rate control. *International Conference on Intelligent Robots and Systems*.